ARTICLE

Filling the gap with a bulky diaryl boron group: fluorinated and non-fluorinated copper pyrazolates fitted with a dimesityl boron moiety on the backbone

Received 00th January 20xx,
Accepted 00th January 20xx

DOI: 10.1039/x0xx00000x

Mukundam Vanga,[†] Benjamin T. Diroll,[‡*] Álvaro R. Muñoz-Castro,[±*] H. V. Rasika Dias[†*]

Successful synthesis of 4-Mes_2B-3,5-$(CF_3)_2$PzH and 4-Mes_2B-3,5-$(CF_3)_2$PzH bearing sterically demanding diarylboron moieties at the pyrazole ring 4-position, and their corresponding copper(I) pyrazole complexes have been reported. They show show visible blue photoluminescence in solution. The X-ray crystal structures revealed that the fluorinated {[4-BMes_2-3,5-$(CF_3)_2$Pz]Cu}$_3$ crystallizes as discrete trinuclear molecules whereas as the non-fluorinated {[4-BMes_2-3,5-$(CH_3)_2$Pz]Cu}$_3$ forms dimers of trimers with two close inter-trimer Cu•••Cu separations. The solid {[4-BMes_2-3,5-$(CF_3)_2$Pz]Cu}$_3$ featuring a sterically confined Cu_3N_6 core displays bright blue phosphorescence while {[4-BMes_2-3,5-$(CH_3)_2$Pz]Cu}$_3$, which is a dimer of trimer, is a red phosphor at room temperature. This work illustrates the modulation of photo-physical properties of metal pyrazolates by adjusting the supporting ligand steric features and introducing secondary diarylboron luminophores. Computational analysis of the structures and photophysical properties of copper complexes are also presented.

Introduction

Trinuclear pyrazolates of copper represent an easily accessible and interesting category of compounds with fascinating photophysical and π-acid/π-base properties, structural features, and diverse applications.[1-5] For example, the d^{10} copper(I) complex {[3,5-$(CF_3)_2$Pz]Cu}$_3$ (**1**, Figure 1)[6] supported by a highly fluorinated pyrazolate forms columns of trimers with close Cu•••Cu separations in crystals, and exhibits bright luminescence in the solid state and glassy solutions upon irradiation with UV radiation that can be fine-and coarse-tuned to multiple bright visible colors by varying the solvent, concentration, temperature, and excitation wavelength.[7, 8] It is also an excellent catalyst for azide-alkyne cycloadditions,[9, 10] permits the separation of olefins from olefin-paraffin mixtures very effectively,[11, 12] and serve as a precursor for nano-clusters of copper.[13] Compound {[3,5-$(CH_3)_2$Pz]Cu}$_3$ (**2**) involving a non-fluorinated pyrazolates is also a photoluminescent solid but exists as discrete dimers of trimers in the solid state with relatively close (2.946 Å), inter-trimer cuprophilic interactions.[8, 14]

Triarylboranes containing dimesitylboron moiety (Mes_2B-, owing to the presence of low-lying empty p_z-orbital on boron and steric bulk; Mes = 2,4,6-$(CH_3)_3C_6H_2$) are widely utilized for applications[15-18] that include the development of photo-luminescent materials, chromophores in OLEDS as well as nonlinear optical materials,[19-24] powerful Lewis acids,[19, 25] isolable radicals,[26-28] and sensors for various analytes including fluoride and cyanide ions.[17, 29-31] Among these, organoboron compounds with heterocyclic linkers such as pyridines, imidazoles, and thiophene, etc., are of significant current interest as they can enhance the electrophilicity at boron, alter luminescence properties, and provide sites for metal ion coordination.[32-37]

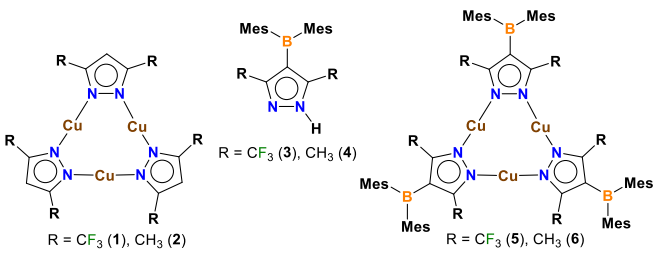

Figure 1. Two representative examples of trinuclear copper pyrazolates {[3,5-$(R)_2$Pz]Cu}$_3$ (**1**, **2**), dimesitylboron decorated

[a.] [†]*Department of Chemistry and Biochemistry, The University of Texas at Arlington, Arlington, Texas 76019, USA; Email: dias@uta.edu*
[b.] *Center for Nanoscale Materials, Argonne National Laboratory, Argonne, Illinois 60439, USA; Email: bdiroll@anl.gov*
[c.] *Facultad de Ingeniería, Arquitectura y Diseño, Universidad San Sebastián, Bellavista 7, Santiago, 8420524, Chile; Email: Alvaro.munozc@uss.cl*
Electronic Supplementary Information (ESI) available: Synthesis, crystallography, physical measurements, computational work, and additional figures. CCDC 2287581-2287582. See DOI: 10.1039/x0xx00000x

pyrazoles 4-BMes$_2$-3,5-(R)$_2$PzH (**3**, **4**), and copper(I) pyrazolates {[4-BMes$_2$-3,5-(R)$_2$Pz]Cu}$_3$ (**5**, **6**). R = CF$_3$, CH$_3$.

Intrigued by the significance of two aforementioned classes of compounds, we set out to develop molecules that incorporate both components. Specifically, we report here the successful synthesis of trinuclear copper(I) complexes {[4-BMes$_2$-3,5-(R)$_2$Pz]Cu}$_3$ (Figure 1, where R = CF$_3$ (**5**), CH$_3$ (**6**)) supported by pyrazolates bearing backbone Mes$_2$B-substituents and their structural and photophysical properties.

Results and discussion

Synthesis and characterization

Dimesitylboron functionalized pyrazoles (i.e., 4-BMes$_2$-3,5-(R)$_2$PzH, R = CF$_3$ (**3**), CH$_3$ (**4**)) utilized in this study have been prepared by a multi-step route starting with 3,5-(CF$_3$)$_2$PzH and 3,5-(CH$_3$)$_2$PzH (Scheme 1). NMR spectroscopic data indicated the successful incorporation of Mes$_2$B moiety to the ligand backbones. Furthermore, in contrast to the boron-free 3,5-(CF$_3$)$_2$PzH and 3,5-(CH$_3$)$_2$PzH, compounds **3** and **4** display bright blue photoluminescence in solution and as solids at room temperature, immediately highlighting the distinct impact of Mes$_2$B- moiety on the photophysical properties of the pyrazoles (Figure S17). Although, the space between two CF$_3$ groups of 3,5-(CF$_3$)$_2$PzH at pyrazolyl ring 4-position has been filled by substituents such as I and NO$_2$,[38] successful installation of a much bulkier Mes$_2$B- group at this position is also noteworthy.

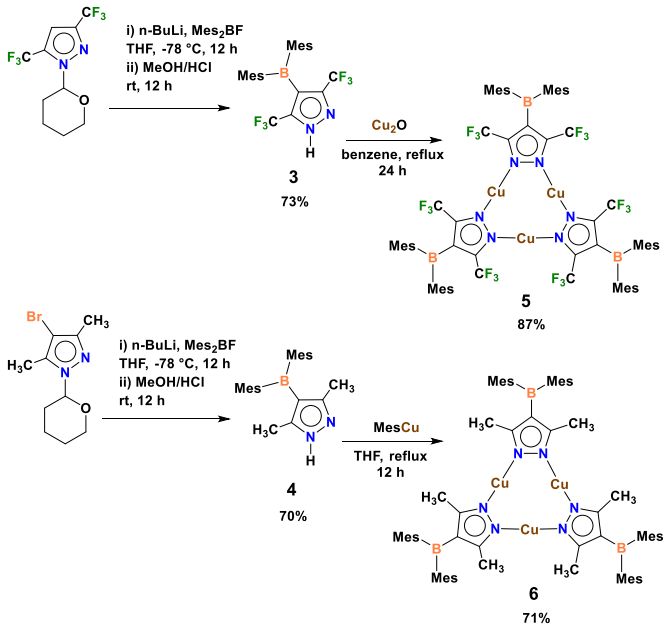

Scheme 1. Synthesis of dimesitylboron decorated pyrazoles **3** and **4**, and copper(I) pyrazolates {[4-BMes$_2$-3,5-(CF$_3$)$_2$Pz]Cu}$_3$ (**5**) and {[4-BMes$_2$-3,5-(CH$_3$)$_2$Pz]Cu}$_3$ (**6**).

The copper complexes {[4-BMes$_2$-3,5-(R)$_2$Pz]Cu}$_3$ (where R = CF$_3$ (**5**), CH$_3$ (**6**)) have been synthesized from their corresponding pyrazoles **3** and **4**, by treating with Cu$_2$O and mesitylcopper(I) and isolated as colorless solids in 87% and 71% yield, respectively (Scheme 1). Compounds **5** and **6** have been fully characterized by NMR spectroscopy, X-ray diffraction techniques, spectrofluorimetric and computational methods.

X-ray crystal structure of **5** and **6** are illustrated in Figure 2. They both feature cyclic trinuclear structures with a nine-membered Cu$_3$N$_6$ core. Selected bond distances and angles of **5** and **6** as well as the related diarylboron free {[3,5-(CF$_3$)$_2$Pz]Cu}$_3$ (**1**), {[3,5-(CH$_3$)$_2$Pz]Cu}$_3$ (**2**) are presented in Table 1. In contrast to **1** which forms columns of trimers with close Cu•••Cu separations (closest at 3.183 Å), {[4-BMes$_2$-3,5-(CF$_3$)$_2$Pz]Cu}$_3$ (**5**) crystallizes as discrete molecules with no close inter-trimer Cu•••Cu contacts. The Mes$_2$B-groups (due to the presence of 3,5-CF$_3$ groups on either side) orient somewhat perpendicular to the Cu$_3$N$_6$ plane (with C$_2$B-CC$_2$ interplanar angles ranging 48.16°-51.98°).

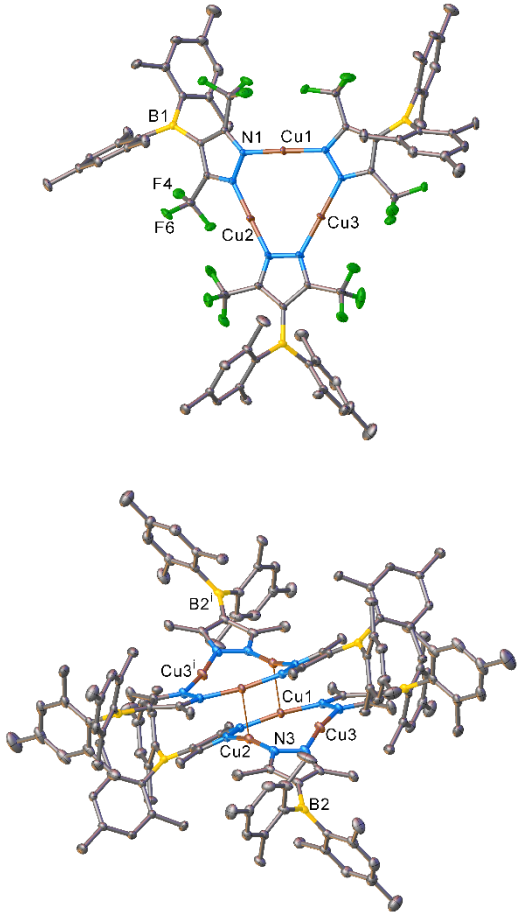

Figure 2. Molecular structures of copper(I) pyrazolate trimer {[4-BMes$_2$-3,5-(CF$_3$)$_2$Pz]Cu}$_3$ (**5**, top) and dimer of trimer {[4-BMes$_2$-3,5-

$(CH_3)_2Pz]Cu\}_3$ (**6**, bottom). Hydrogen atoms and solvents of crystallization have been omitted for clarity.

Table 1. Selected bond distances (Å) and angles (°) for $\{[3,5\text{-}(CF_3)_2Pz]Cu\}_3$ (**1**), $\{[3,5\text{-}(CH_3)_2Pz]Cu\}_3$ (**2**), $\{[4\text{-}BMes_2\text{-}3,5\text{-}(CF_3)_2Pz]Cu\}_3$ (**5**) and $\{[4\text{-}BMes_2\text{-}3,5\text{-}(CH_3)_2Pz]Cu\}_3$ (**6**), and lifetimes of photoluminescence. The Cu•••Cu$^{(inter)}$ and Cu•••Cu$^{(intra)}$ refer to shortest inter- and intra-trimer Cu•••Cu separations.

	5	**1**	**6**	**2**
Cu-N	1.8601(15)-1.8752(14)	1.855(2)-1.863(2)	1.8520(15)-1.8665(17)	1.845(4)-1.858(4)
Cu•••Cu$^{(intra)}$	3.184	3.218	3.111	3.195
Cu•••Cu$^{(inter)}$	> 8.09	3.813	3.007	2.946
N-Cu-N	174.18(7)-178.99(7)	178.39(10)-178.58(10)	165.45(7)-172.63(7)	173.4(2)-175.3(2)
B-C(Pz)	1.573(3)-1.581(2)		1.532(3)-1.540(3)	
τ_{PL}, 295K	1.39(1) ns	52.6(8) µs	16.1(1) µs	50.1(29) µs
ref	this work	[8]	this work	[14]

We evaluated the rotation barrier related to the Mes_2B-Pz dihedral angle in the $\{[4\text{-}BMes_2\text{-}3,5\text{-}(R)_2Pz]Cu\}_3$ systems (R = CF_3, CH_3, H) computationally, which is found to be largely dependent on the characteristics of the 3,5-$(R)_2$ groups. The rotation profiles denote the sizable steric hindrance introduced by the $–CF_3$ group, where angles from 0-30° and 70-90° are not allowed (Figure 3). This contrast with the situation found in the $–CH_3$ species, for which rotational energies lie below 50 kcal·mol^{-1} for angles between 0° and 80°, and even lower for the hypothetical 3,5-$(H)_2$ counterpart. The optimized Mes_2B-Pz dihedral angles for **5** and **6** are 46.2 and 27.3°, respectively, which compares well to the experimental observations. For comparison, the respective dihedral angle for the 3,5-$(H)_2$ analog is 18.3° in the optimized structure. The large barrier noted above for **5** hinders close approach of neighboring dimers and dimer of trimer formation which provides a rare opportunity to observe the luminescence of "confined" trinuclear copper moieties in the absence of inter-trimer Cu•••Cu interactions.[39] Such contacts are often attributed to higher-wavelength emissions resulting from exited state formation of $*[Cu_3]_2$ excimers with shorter Cu•••Cu interactions in trinuclear copper pyrazolates.[2, 8, 39-42] The three Mes_2B-moieties of two neighboring copper-trimers form walls of a pocket between two Cu_3N_6 units which is occupied in crystals of **5** by *n*-heptane molecules (solvent of crystallization, Figures S11-S13). The Cu-N distances of **5** are similar to those observed for **1**. The N-Cu-N angles are close to linear and the Cu_3N_6 core is only slightly twisted from planarity.

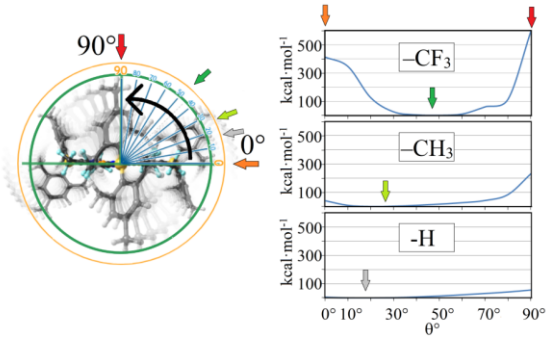

Figure 3. Relative energy profile in relation to the Mes_2B-Pz dihedral angle variation in $\{[4\text{-}BMes_2\text{-}3,5\text{-}(R)_2Pz]Cu\}_3$ systems (R = CF_3 (**5**), CH_3 (**6**), H).

The non-fluorinated copper adduct $\{[4\text{-}BMes_2\text{-}3,5\text{-}(CH_3)_2Pz]Cu\}_3$ (**6**) crystallizes as dimers of trimers with two close inter-trimer Cu•••Cu separations (3.0066(3) Å) but they are longer than the summed Bondi's van der Waals radii (r_{vdW}) of adjacent Cu atoms (2.80 Å).[43] However, the trimer units seem to curved away from each other to facilitate these cuprophilic contacts.[44] The trimer of dimer sits on a center of inversion and the Cu_6 fragment adopts a "Z-shape". For comparison, $\{3,5\text{-}(CH_3)_2PzCu\}_3$ (**2**) also crystallizes as dimers of trimers with even closer Cu•••Cu contacts (2.946 Å)[8, 14] but features a more flattened chair (a "lazy boy" recliner) arrangement of the Cu_6 unit. The Mes_2B-groups (due to the presence of smaller pyrazolyl ring 3,5-CH_3 groups on either side) orient relatively more coplanar fashion to the Cu_3N_6 plane (in comparison to **5**, with smaller $C_2B\text{-}CC_2$ interplanar angles with a range 22.22°-36.39°), in good agreement with the computed value noted above. The six Mes_2B-groups of neighboring dimers of trimers also form pockets but they are relatively shallow and occupied by mesityl moieties of Mes_2B (Figures S14-S16), while solvent of crystallization (*n*-heptane) is also present, but on sides of the molecules of **6**. The B-C(Pz) distances of **6** (Table 1) are shorter than those of **5**, perhaps indicating greater π-overlap between the empty p_z of boron with pyrazolyl ring system. The N-Cu-N angles range from 165.45(7)°-172.63(7)°, and are more acute that those of **2**. Larger deviation from linearity is a result of distortions caused by dimer of trimer formation. Longer Cu-N distances are associated with the copper atoms that participate in the inter-trimer Cu•••Cu interactions.

Photophysical properties

Absorption and emission of Mes_2B-functionalized pyrazoles **3** & **4** and their copper(I) complexes **5** & **6** (vacuum dried to remove any solvents) were studied in chloroform at room temperature. Emission and lifetime properties were also explored at room temperature and 80 K, both in chloroform and in the solid state (Table S7). All show absorption maxima in 308-332 nm range (in chloroform). Chloroform solutions of **3**, **4** and the corresponding copper complexes **5, 6** show blue emission with fast lifetimes of 0.9-3.6 ns. Measurements at 80

K show a shift to longer wavelength, with well-defined vibrational bands, but reduced photoluminescence lifetimes, compared to data at room temperature, indicating emission still derives from a singlet state. As explained below, this blue emission is due to the impact of Mes_2B group (see also Figure S17). In the solid state at room temperature, **3**, **4** and complex **5** also show a blue emission but compound **6** the emits a notably different and captivating red color (Figure 4). Not only is the powder form of **6** substantially different in emission spectrum from **3**, **4**, or **5**, the lifetime of photoluminescence is also 10^4 times longer, with a room temperature lifetime of 16.1 µs, compared to the 1.4-2.3 ns lifetimes of the other compounds in powder form. At 80 K, the emission lifetime of **6** elongates further to 38.9 µs**.** The elongated lifetime of the redshifted emission of **6** in the solid state confirms the origin is from a triplet (i.e., phosphorescence) rather than a singlet state which prevails in the isolated molecules or solids of **3**, **4**, or **5.** The difference in the photoluminescence behavior between the two copper(I) complexes is attributable to the absence or existence of close inter-trimer Cu•••Cu contacts in **5** and **6**, respectively, in solid powders, with the cuprophilic interactions of **6** driving the emergence of a triplet emission.

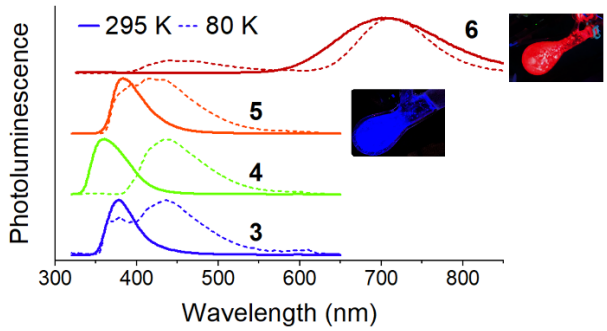

Figure 4. Photoluminescence of powders of dimesitylboron decorated pyrazoles 4-$BMes_2$-3,5-$(R)_2PzH$ (**3** and **4,** R = CF_3, CH_3), and copper(I) pyrazolates $\{[4\text{-}BMes_2\text{-}3,5\text{-}(R)_2Pz]Cu\}_3$ (**5** and **6**, R = CF_3, CH_3) at 295 K (solid lines) and 80 K (dashed lines). Excitation at 300 nm. Insets: photographs show compound **5** (blue) and **6** (red) under UV illumination at 295 K.

To further rationalize the observed optical properties, DFT calculations were carried out on Mes_2B-decorated ligands **3** and **4**, and the related copper(I) complexes **5** and **6**. Interestingly, the free ligands and copper complexes share a similar absorption band, with a related emission maximum. The highest-occupied and lowest-unoccupied orbital gap (HOMO-LUMO gap) remains similar between the isolated ligands and copper complexes. The calculated absorption maxima for the isolated ligands **3** and **4** are located at 376 and 343 nm (Figure S27), which are in line to the experimentally observed values of 332 and 308, respectively, within the method error, involving HOMO to LUMO transitions, attributable to charge transfer from mesityl to p_z-B orbital. For copper complexes **5** and **6**, the calculated absorption maxima are located at 368 and 340 nm (cf. 327 and 314 nm, experimentally) of pyrazole → p_z-B and mesityl → p_z-B character, respectively, corresponding to intra-ligand charge transfer (ILCT) similar to those observed for free ligands (Figure S27).

The related $T_1 \rightarrow S_0$ emission of both isolated ligands and their isolated trinuclear copper complexes is calculated at 434 and 435 nm for **3** and **4** ligands, and 411 and 435 nm for **5** and **6**, respectively. The structural distortions between T_1 and S_0 states are mainly correspond to small variations in the Mes_2B-Pz dihedral angle.

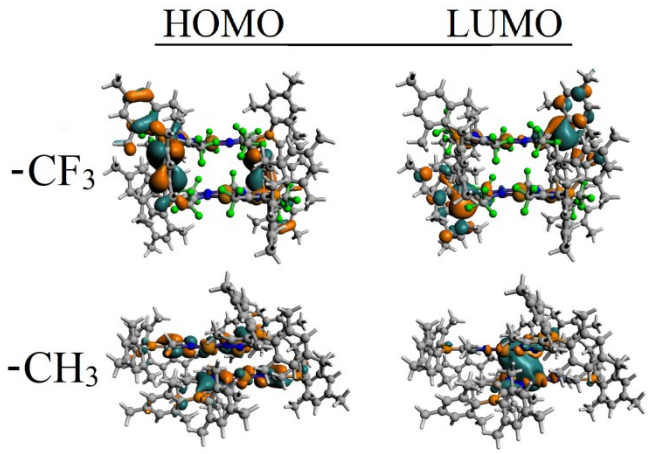

Figure 5. Side view of the HOMO and LUMO isosurfaces for stacked dimers of $\{[4\text{-}BMes_2\text{-}3,5\text{-}(CF_3)_2Pz]Cu\}_3$ (**5**) and $\{[4\text{-}BMes_2\text{-}3,5\text{-}(CH_3)_2Pz]Cu\}_3$ (**6**) (i.e., $(\mathbf{5})_2$ and $(\mathbf{6})_2$), related to the radiative $T_1 \rightarrow S_0$ decay.

The crystal structures revealed a stacked aggregation involving a dimer of trimer for **6**, and discrete trinuclear copper units for **5** (Figure 2). The optimized structure (solvent free) for the stacked dimer of **6** shows intermolecular Cu•••Cu separations of 2.967 Å, denoting cuprophilic interactions, which compares well to the experimental data (3.007 Å).[45] Calculations on the hypothetical dimer of trimer of **5** displayed longer Cu•••Cu separations of 4.947 Å. Further evaluation of the interaction energy between two copper trimers shows values of -99.2 and -76.3 kcal/mol, where the repulsion term related to steric hindrance, is notably enhanced in hypothetical $(\mathbf{5})_2$, indicating that closer approach of copper sites of two trimers units to form Cu•••Cu interactions is prevented by near vertically aligned Mes_2B- (at 48.0°) groups and CF_3 groups.

Solid-state emissions of the stacked models were also evaluated using X-ray data (without the solvents of crystallization). For the dimer of **5**, the $T_1 \rightarrow S_0$ emission calculated at 431 nm is related to the mesityl → p_z-B transition character (Figure 5) ascribed to a LUMO→HOMO manifold character (97%), similar to that of the metal-free ligand. In contrast, the non-fluorinated counterpart (dimer of **6**) with close Cu•••Cu contacts exhibits an emission process ascribable

to the $[Cu_3]$-$[Cu_3]$ core, leading to an increase in the intermolecular bonding character and a notably shorter inter-trimer Cu-Cu distance (2.688 Å) in the excited T_1 state, similar to previously reported dimers of trinuclear copper species (Figure S20).[8, 40, 41] The calculated $T_1 \rightarrow S_0$ emission of 623 nm is similar to that observed experimentally with a peak at 704 nm, which is of 98% LUMO→HOMO character. Overall, the steric contributions introduced by pyrazolyl ring 3,5–CF_3 and 4-Mes_2B- groups strongly hinder copper trimer aggregation, and the subsequent emission characteristics with long lifetimes, illustrating a way to control photo-physical properties of these copper complexes by modulating ligand bulk. Such remote steric effect driven control of the photoluminescence is a topic of current interest, and has been reported in a tetranuclear copper(I) pyrazolates associated with deep-blue emitting phosphors.[46]

Conclusions

In summary, we successfully installed a Mes_2B- group onto pyrazole ring 4-position of 3,5-$(CF_3)_2$PzH and 3,5-$(CH_3)_2$PzH affording **3** and **4**. These novel diarylboron decorated pyrazoles and their pyrazolates complexes copper, **5** and **6** show visible blue photoluminescence in solution in contrast to their Mes_2B-free counterparts. Emissions are a result of intra-ligand charge transfer (ILCT) involving p_z-orbital on boron. The fluorinated trinuclear copper complex **5** with a sterically confined Cu_3N_6 core is a bright blue phosphor, in contrast to the diarylboron free **1** which is a deep orange emitter[6] with close inter-trimer Cu•••Cu separations. Non-fluorinated compound **6**, which forms dimers of trimers in solid-state is a strikingly bright red phosphor (cf. yellow emitter **2**)[6] at room temperature. This work illustrates a way to tune photo-physical properties of coinage metal pyrazolates by modulating ligand steric features and through secondary luminophores. We are exploring several applications and other metal analogues of these materials.

Experimental section

Materials and general methods

All manipulations were carried out under an atmosphere of purified nitrogen using standard Schlenk techniques or in a MBraun glovebox equipped with a -25 °C refrigerator. Solvents were purchased from commercial sources, purified prior to use. Glassware was oven dried overnight at 150 °C. NMR spectra were acquired at 25 °C, on a JEOL Eclipse 500 spectrometer. NMR spectra were acquired at 25 °C (unless noted) on a JEOL Eclipse 500 spectrometer (^{1}H, 500 MHz; ^{13}C, 126 MHz; ^{19}F, 471 MHz) and all the spectral data were processed on MNova. ^{19}F NMR values were referenced to external $CFCl_3$. ^{1}H and ^{13}C NMR spectra were referenced internally to solvent signals ($CDCl_3$: 7.26 ppm for ^{1}H NMR, 77.16 ppm for ^{13}C NMR), or externally to $SiMe_4$ (0 ppm). Abbreviations used for signal assignments: Me = Methyl, Mes= Mesityl, s = singlet, q = quartet, brs = broad singlet. NMR solvents were purchased from Cambridge Isotopes Laboratories and used as received. High-resolution (HR) mass spectra were recorded at Shimadzu Center Laboratory for Biological Mass Spectrometry at UTA. Heating was accomplished by either a heating mantle or silicone oil bath. Purification of reaction products was carried out by flash column chromatography using silica gel 60 (230-400 mesh). TLC visualization was accompanied with UV light. The 1-(tetrahydro-2H-pyran-2-yl)-3,5-bis(trifluoromethyl)-1H-pyrazole,[47] 4-bromo-3,5-dimethyl-1-(tetrahydro-2H-pyran-2-yl)-1H-pyrazole,[48] and Mes_2BF[49] were prepared using literature procedures. All other reactants and reagents were purchased from commercial sources.

Synthesis of [4-$BMes_2$-3,5-$(CF_3)_2$Pz]H **(3)**

To a solution of 1-(tetrahydro-2H-pyran-2-yl)-3,5-bis(trifluoromethyl)-1H-pyrazole (4.00 g, 13.9 mmol) in anhydrous THF (100 mL) at -78 °C, a solution of *n*-BuLi (9.5 mL, 1.6 M in hexane, 15.27 mmol) was added. The mixture was stirred for 45 minutes. Subsequently, fluorodimesitylborane (4.09 g, 15.27 mmol) in anhydrous THF (40 mL) at -78 °C was added. The mixture was then warmed to room temperature and stirring continued for 12 hours. Deionized H2O (100 mL) was added, and the mixture was extracted with ethyl acetate (3 × 30 mL). The combined organic layers were washed with a brine solution, dried over anhydrous Na_2SO_4, and evaporated to dryness under reduced pressure. The resulting solid was dissolved in MeOH (100 mL), and conc. HCl (11.5 mL) was slowly added. The mixture was stirred for 12 hours. The reaction mixture was neutralized with saturated aqueous sodium bicarbonate, and the aqueous layer was extracted with ethyl acetate. The combined organic layers were washed again with a brine solution, dried over anhydrous Na_2SO_4, and evaporated to dryness under reduced pressure. The resulting solid was purified using silica gel column chromatography with ethyl acetate and n-hexanes as eluents to obtain [4-$BMes_2$-3,5-$(CF_3)_2$Pz]H as a white solid. Yield: 4.6 g (73%). ^{1}H NMR (500 MHz, $CDCl_3$) : δ (ppm) 6.76 (s, 4H, ArH), 2.28 (s, 6H, *p*-CH_3^{Mes}), 1.97 (s, 12H *o*-CH_3^{Mes}). ^{13}C{^{1}H} NMR (126 MHz, $CDCl_3$): δ (ppm) 141.28 (brs), 141.04, 141.49, 128.65, 128.43, 120.06 (q, $^1J_{C\text{-}F}$ = 270.9 Hz, CF_3), 23.29 (*o*-CH_3^{Mes}), 22.50 (*o*-CH_3^{Mes}), 21.43 (*p*-CH_3^{Mes}). ^{19}F NMR (471 MHz, $CDCl_3$): δ (ppm) -59.27 (s). HR-MS [ESI, positive ion mode ESI-TOF]: m/z for $C_{23}H_{24}B_1F_6N_2$ $[M+H]^+$ calcd: 453.1937. Found: 453.1933.

Synthesis of 4-$BMes_2$-3,5-$(CH_3)_2$PzH **(4)**

To a solution of 4-bromo-3,5-dimethyl-1-(tetrahydro-2H-pyran-2-yl)-1H-pyrazole (3.5 g, 13.5 mmol) in anhydrous THF (100 mL) at -78 °C, a solution of *n*-BuLi (8.7 mL, 1.6 M in hexane, 13.91 mmol) was added. The mixture was stirred for 45 minutes. Subsequently, fluorodimesitylborane (3.80 g, 14.18 mmol) in anhydrous THF (40 mL) at -78 °C was added. The mixture was then warmed to room temperature and stirring continued for 12 hours. Deionized H_2O (100 mL) was

added, and the mixture was extracted with ethyl acetate (3 × 30 mL). The combined organic layers were washed with a brine solution, dried over anhydrous Na_2SO_4, and evaporated to dryness under reduced pressure. The resulting solid was dissolved in MeOH (100 mL), and conc. HCl (11.5 mL) was slowly added. The mixture was stirred for 12 hours. The reaction mixture was neutralized with saturated aqueous sodium bicarbonate, and the aqueous layer was extracted with ethyl acetate. The combined organic layers were washed again with a brine solution, dried over anhydrous Na_2SO_4, and evaporated to dryness under reduced pressure. The resulting solid was purified using silica gel column chromatography with ethyl acetate and n-hexanes as eluents to obtain 4-$BMes_2$-3,5-$(CH_3)_2$PzH as a white solid. Yield: 3.26 g (70%). ^{1}H NMR (500 MHz, $CDCl_3$): δ (ppm) 6.78 (s, 4H, ArH), 2.28 (s, 6H, *o*-CH_3^{Mes}), 2.10 (s, 12H, *p*-CH_3^{Mes}), 1.86 (s, 6H, CH_3^{Pz}). ^{13}C{^{1}H} NMR (126 MHz, $CDCl_3$): δ (ppm) 151.94, 142.43, 139.77, 138.11, 128.35, 121.94, 22.86 (CH_3^{Mes}), 21.28 (CH_3^{Mes}), 12.83 (CH_3^{Pz}). HR-MS [ESI, positive ion mode ESI-TOF]: m/z for $C_{23}H_{30}B_1N_2$ $[M+H]^+$ calcd: 345.2502. Found: 345.2497.

Synthesis of {[4-$BMes_2$-3,5-$(CF_3)_2$Pz]Cu}$_3$ **(5)**

Anhydrous benzene (60 mL) and acetonitrile (0.5 mL) were added to a mixture of Cu_2O (0.22 g, 1.53 mmol) and [4-$BMes_2$-3,5-$(CF_3)_2$Pz]H (1.26 g, 2.79 mmol) in a 100 mL Schlenk flask under an inert atmosphere. The reaction mixture was then heated to reflux for 12 hours. After cooling to room temperature, the solution was filtered through a bed of Celite to remove some insoluble material. The filtrate was collected, and the solvent was removed under reduced pressure to obtain {[4-$BMes_2$-3,5-$(CF_3)_2$Pz]Cu}$_3$ as an off-white powder. This powder was then vacuum-dried at 80 °C for 5 hours to remove trace solvents. X-ray quality crystals were grown from a solution of hot heptane through slow cooling. Yield: 1.25 g (87%) (based on the amount of pyrazole used). ^{1}H NMR (500 MHz, $CDCl_3$): δ (ppm) 6.75 (s, 4H, ArH), 2.27 (s, 6H, *p*-CH_3^{Mes}), 1.95 (s, 12H, *o*-CH_3^{Mes}). ^{13}C{^{1}H} NMR (126 MHz, $CDCl_3$): δ (ppm) 145.98 (q, $^2J_{C\text{-}F}$ = 34.0 Hz, C-3/C-5), 141.44, 141.28, 140.33, 128.66, 124.58, 120.32 (q, $^1J_{C\text{-}F}$ = 271.7 Hz, CF_3), 23.38 (*o*-CH_3^{Mes}), 22.68 (*o*-CH_3^{Mes}), 21.45 (*p*-CH_3^{Mes}). ^{19}F NMR (471 MHz, $CDCl_3$): δ (ppm) -57.68 (s).

Synthesis of {[4-$BMes_2$-3,5-$(CH_3)_2$Pz]Cu}$_3$ **(6)**

To a mixture of MesCu (0.44 g, 2.41 mmol) and [4-$BMes_2$-3,5-$(CH_3)_2$Pz]H in a 100 mL Schlenk flask, anhydrous THF was added under an inert atmosphere. The reaction mixture was then heated to reflux for 12 hours. After cooling, the solution was filtered through a bed of celite to remove any insoluble material. The filtrate was collected, and the solvent was removed under reduced pressure. The resulting residue was dissolved in a minimum amount of anhydrous dichloromethane, and then excess anhydrous hexane was added to precipitate the compound. After allowing the precipitate to settle at the bottom of the Schlenk flask, the supernatant liquid was carefully removed using a filter cannula. The precipitated compound was then dried under vacuum to obtain the {[4-$BMes_2$-3,5-$(CH_3)_2$Pz]Cu}$_3$ as an off-white powder. Subsequently, it was vacuum-dried at 80 °C for 5 hours to remove trace solvent. Yield: 0.7 g (71%) (based on the amount of pyrazole used). ^{1}H NMR (500 MHz, $CDCl_3$): δ (ppm) 6.78 (s, 4H, ArH), 2.28 (s, 6H, *o*-CH_3^{Mes}), 2.10 (s, 12H, *p*-CH_3^{Mes}), 1.90 (s, 6H, CH_3^{Pz}). ^{13}C{^{1}H} NMR (126 MHz, $CDCl_3$): δ (ppm) 157.59, 142.88, 139.81, 137.91, 128.30, 121.72, 22.90 (CH_3^{Mes}), 21.30(CH_3^{Mes}), 14.77 (CH_3^{Pz}).

X-ray Data Collection and Structure Determinations

A suitable crystal covered with a layer of hydrocarbon/Paratone-N oil was selected and mounted on a Cryo-loop, and immediately placed in the low temperature nitrogen stream. The X-ray intensity data were measured at 100(2) K (unless otherwise noted) on a Bruker D8 Quest equipped with a PHOTON II 7 CPAD detector and an Oxford Cryosystems 700 series cooler, a Triumph monochromator, and a Mo Kα fine-focus sealed tube (λ = 0.71073 Å). Intensity data were processed using the Bruker Apex program suite. Absorption corrections were applied by using SADABS.[50] Initial atomic positions were located by SHELXT,[51] and the structures of the compounds were refined by the least-squares method using SHELXL[52] within Olex2 GUI.[53] All the non-hydrogen atoms were refined anisotropically. Hydrogen atoms were included at calculated positions and refined using appropriate riding models. X-ray structural figures were generated using Olex2. Compound {[4-($BMes_2$)-3,5-$(CF_3)_2$Pz]Cu}$_3$ (**5**) crystallizes with 1.5 molecules of *n*-heptane in the asymmetric unit (residing above and below the Cu_3N_6 core). Heptanes show positional disorder over two positions. Fluorine atoms of one of the CF_3 groups also show positional disorder over two positions. These disorders were modelled satisfactorily. Copper complex {[4-($BMes_2$)-3,5-$(CH_3)_2$Pz]Cu}$_3$ (**6**) crystallizes with one molecule of *n*-heptane in the asymmetric unit which shows positional disorder over two positions. It was also modelled satisfactorily. The {[4-($BMes_2$)-3,5-$(CH_3)_2$Pz]Cu}$_3$ forms dimers of trimers with two Cu•••Cu contacts. CCDC 2287581-2287582 files contain the supplementary crystallographic data that have been deposited at the Cambridge Crystallographic Data Centre (CCDC).

Optical data collection.

Absorption spectra of the samples dissolved as dilute solutions in chloroform were performed using a Cary-50 spectrometer. Photoluminescence spectrum measurements were performed using a Horiba Jobin-Yvon FL-3 fluorimeter. Time-resolved data for the samples was collected by converting the output of a 2 khz, 35 fs Ti: sapphire laser into 325 nm pulses using an optical parametric amplifier. Light emission from the samples was measured using a streak camera (Hamamatsu). Data fitting occurred after integrating across the full spectrum. Measurements of solutions at ~80 K were performed by emersion of the samples loaded into NMR

tubes in liquid nitrogen. Powder samples were measured in a Janis cryostat.

Computational details

Calculations were performed via density functional theory with Slater-type orbitals (STO) of triple-zeta quality basis set plus two polarization functions (TZ2P), by using the ADF2019 suite.[54] Becke exchange and the Perdew correlation functional (BP86),[55, 56] in conjunction with the Grimme's empirical dispersion correction with the Becke-Johnson damping functions, D3(BJ), were employed for all the calculations.[57] The frozen core approximation was applied to the [$1s^2$-$3p^6$] shell for Cu, [$1s^2$] for B, C, N, and F, leaving the remaining electrons to be treated variationally. Calculated geometries were optimized without any symmetry constraints via the analytical energy gradient method implemented by Versluis and Ziegler,[58] with an energy convergence criterion of 10^{-4} Hartree, gradient convergence of 10^{-3} Hartree/Å, and radial convergence of 10^{-2} Å. Optical properties were calculated by using Time-Dependent DFT (TDDFT) via the exchange-correlation functional of Van Leeuwen and Baerends[59] with TZ2P basis set. Evaluation of the optical emission properties was achieved by optimizing the emissive T_1 state enabling calculation of the $T_1 \rightarrow S_0$ radiative decay by using TDDFT at the T_1 geometry.[60]

Energy decomposition analysis was achieved within the Ziegler-Rauk scheme,[61] where the overall interaction energy (ΔE_{int}) is further dissected in chemically meaningful terms,[62] accounting for four-electrons two-orbital repulsion between occupied orbitals from the different fragments (ΔE_{Pauli}), the electrostatic interaction character (ΔE_{elstat}), the orbital interaction (Δ_{orb}), and the dispersion type interactions (ΔE_{disp}) from the pair-wise correction from Grimme and the Becke-Johnson (BJ) damping function (D3-BJ).

Conflicts of interest

There are no conflicts to declare.

Acknowledgements

This material is based upon work supported by the National Science Foundation under grant number CHE-1954456. A.M.-C. thanks the financial support from FONDECYT 1221676. Work performed at the ANL Center for Nanoscale Materials was supported by the U.S. DOE, Office of Basic Energy Sciences, under Contract No. DE-AC02-06CH11357.

Notes and references

1. J. Zheng, Z. Lu, K. Wu, G.-H. Ning and D. Li, *Chem. Rev.*, 2020, **120**, 9675-9742.
2. R. Galassi, M. A. Rawashdeh-Omary, H. V. R. Dias and M. A. Omary, *Comments Inorg. Chem.*, 2019, **39**, 287-348.
3. J. Zheng, H. Yang, M. Xie and D. Li, *Chem. Commun.*, 2019, **55**, 7134-7146.
4. W.-J. Tang, H. Yang, S.-K. Peng, Z.-M. Xiao, G.-Q. Huang, J. Zheng and D. Li, *Inorg. Chem. Front.*, 2023, **10**, 2594-2606.
5. R.-Q. Xia, J. Zheng, R.-J. Wei, J. He, D.-Q. Ye, M.-D. Li, G.-H. Ning and D. Li, *Inorg. Chem. Front.*, 2022, **9**, 2928-2937.
6. H. V. R. Dias, S. A. Polach and Z. Wang, *J. Fluor. Chem.*, 2000, **103**, 163-169.
7. H. V. R. Dias, H. V. K. Diyabalanage, M. A. Rawashdeh-Omary, M. A. Franzman and M. A. Omary, *J. Am. Chem. Soc.*, 2003, **125**, 12072-12073.
8. H. V. R. Dias, H. V. K. Diyabalanage, M. G. Eldabaja, O. Elbjeirami, M. A. Rawashdeh-Omary and M. A. Omary, *J. Am. Chem. Soc.*, 2005, **127**, 7489-7501.
9. A. A. Titov, V. A. Larionov, A. F. Smol'yakov, M. I. Godovikova, E. M. Titova, V. I. Maleev and E. S. Shubina, *Chem. Commun.*, 2019, **55**, 290-293.
10. D. Parasar, T. T. Ponduru, A. Noonikara-Poyil, N. B. Jayaratna and H. V. R. Dias, *Dalton Trans.*, 2019, **48**, 15782-15794.
11. D. Parasar, A. H. Elashkar, A. A. Yakovenko, N. B. Jayaratna, B. L. Edwards, S. G. Telfer, H. V. R. Dias and M. G. Cowan, *Angew. Chem., Int. Ed.*, 2020, **59**, 21001-21006.
12. A. H. Elashkar, D. Parasar, A. Muñoz-Castro, C. M. Doherty, M. G. Cowan and H. V. R. Dias, *ChemPlusChem*, 2021, **86**, 364-372.
13. S.-K. Peng, H. Yang, D. Luo, M. Xie, W.-J. Tang, G.-H. Ning and D. Li, *Inorg. Chem. Front.*, 2022, **9**, 5327-5334.
14. M. K. Ehlert, S. J. Rettig, A. Storr, R. C. Thompson and J. Trotter, *Can. J. Chem.*, 1990, **68**, 1444-1449.
15. L. Ji, S. Griesbeck and T. B. Marder, *Chem. Sci.*, 2017, **8**, 846-863.
16. F. Jäkle, *Chem. Rev.*, 2010, **110**, 3985-4022.
17. C. R. Wade, A. E. J. Broomsgrove, S. Aldridge and F. P. Gabbaï, *Chem. Rev.*, 2010, **110**, 3958-3984.
18. Z. M. Hudson and S. Wang, *Acc. Chem. Res.*, 2009, **42**, 1584-1596.
19. Y. Cao, J. K. Nagle, M. O. Wolf and B. O. Patrick, *J. Am. Chem. Soc.*, 2015, **137**, 4888-4891.
20. W. L. Jia, X. D. Feng, D. R. Bai, Z. H. Lu, S. Wang and G. Vamvounis, *Chem. Mater.*, 2005, **17**, 164-170.
21. G. Turkoglu, M. E. Cinar and T. Ozturk, *Molecules*, 2017, **22**, 1522.
22. C. Branger, M. Lequan, R. M. Lequan, M. Barzoukas and A. Fort, *J. Mater. Chem.*, 1996, **6**, 555-558.
23. Z. Yuan, C. D. Entwistle, J. C. Collings, D. Albesa-Jove, A. S. Batsanov, J. A. K. Howard, N. J. Taylor, H. M. Kaiser, D. E. Kaufmann, S.-Y. Poon, W.-Y. Wong, C. Jardin, S. Fathallah, A. Boucekkine, J.-F. Halet and T. B. Marder, *Chem. Eur. J.*, 2006, **12**, 2758-2771.
24. R. P. Nandi, N. K. Kalluvettukuzhy, S. Pagidi and P. Thilagar, *Inorg. Chem.*, 2023, **62**, 1122-1134.
25. M. Schulte and F. P. Gabbai, *Chem. Eur. J.*, 2002, **8**, 3802-3807.
26. S. I. Weissman and H. Van Willigen, *J. Am. Chem. Soc.*, 1965, **87**, 2285-2286.
27. C.-W. Chiu and F. P. Gabbai, *Angew. Chem., Int. Ed.*, 2007, **46**, 1723-1725.
28. N. Yuan, W. Wang, Z. Wu, S. Chen, G. Tan, Y. Sui, X. Wang, J. Jiang and P. P. Power, *Chem. Commun.*, 2016, **52**, 12714-12716.

29. Y. Kim and F. P. Gabbai, *J. Am. Chem. Soc.*, 2009, **131**, 3363-3369.
30. T. W. Hudnall and F. P. Gabbaie, *J. Am. Chem. Soc.*, 2007, **129**, 11978-11986.
31. G. Zhou, M. Baumgarten and K. Muellen, *J. Am. Chem. Soc.*, 2008, **130**, 12477-12484.
32. Y. Sun and S. Wang, *Inorg. Chem.*, 2010, **49**, 4394-4404.
33. I. Avinash, S. Parveen and G. Anantharaman, *Inorg. Chem.*, 2020, **59**, 5646-5661.
34. Z. Zhao, X. Yin, T. Peng, N. Wang and S. Wang, *Inorg. Chem.*, 2020, **59**, 7426-7434.
35. Z. M. Hudson and S. Wang, *Dalton Trans.*, 2011, **40**, 7805-7816.
36. Y.-L. Rao, D. Schoenmakers, Y.-L. Chang, J.-S. Lu, Z.-H. Lu, Y. Kang and S. Wang, *Chem. Eur. J.*, 2012, **18**, 11306-11316, S11306/11301-S11306/11360.
37. G. R. Kumar, S. K. Behera and P. Thilagar, *Dalton Trans.*, 2019, **48**, 6817-6823.
38. A. Maspero, G. B. Giovenzana, D. Monticelli, S. Tagliapietra, G. Palmisano and A. Penoni, *J. Fluor. Chem.*, 2012, **139**, 53-57.
39. F. Gong, Q. Wang, J. Chen, Z. Yang, M. Liu, S. Li, G. Yang, L. Bai, J. Liu and Y. Dong, *Inorg. Chem.*, 2010, **49**, 1658-1666.
40. M. A. Omary, M. A. Rawashdeh-Omary, M. W. A. Gonser, O. Elbjeirami, T. Grimes, T. R. Cundari, H. V. K. Diyabalanage, C. S. P. Gamage and H. V. R. Dias, *Inorg. Chem.*, 2005, **44**, 8200-8210.
41. I. I. Vorontsov, A. Y. Kovalevsky, Y.-S. Chen, T. Graber, M. Gembicky, I. V. Novozhilova, M. A. Omary and P. Coppens, *Phys. Rev. Lett.*, 2005, **94**, 193003.
42. T. Grimes, M. A. Omary, H. V. R. Dias and T. R. Cundari, *J. Phys. Chem. A*, 2006, **110**, 5823-5830.
43. S. Alvarez, *Dalton Trans.*, 2013, **42**, 8617-8636.
44. N. B. Jayaratna, M. M. Olmstead, B. I. Kharisov and H. V. R. Dias, *Inorg. Chem.*, 2016, **55**, 8277-8280.
45. N. V. S. Harisomayajula, S. Makovetskyi and Y.-C. Tsai, *Chem. Eur. J.*, 2019, **25**, 8936-8954.
46. Y. Watanabe, B. M. Washer, M. Zeller, S. Savikhin, L. V. Slipchenko and A. Wei, *J. Am. Chem. Soc.*, 2022, **144**, 10186-10192.
47. I. I. Gerus, R. X. Mironetz, I. S. Kondratov, A. V. Bezdudny, Y. V. Dmytriv, O. V. Shishkin, V. S. Starova, O. A. Zaporozhets, A. A. Tolmachev and P. K. Mykhailiuk, *J. Org. Chem.*, 2012, **77**, 47-56.
48. A. A. Protter, P. Y. Lum, G. R. Luedtke, Preparation of the derivatives of piperlongumine and their medical applications, US Patent 20200377510, 2020.
49. E. Le Coz, J. Hammoud, T. Roisnel, M. Cordier, V. Dorcet, S. Kahlal, J.-F. Carpentier, J.-Y. Saillard and Y. Sarazin, *Chem. Eur. J.*, 2021, **27**, 11966-11982.
50. L. Krause, R. Herbst-Irmer, G. M. Sheldrick and D. Stalke, *J. Appl. Crystallogr.*, 2015, **48**, 3-10.
51. G. Sheldrick, *Acta Crystallogr. Sect. A: Found. Adv.*, 2015, **71**, 3-8.
52. G. Sheldrick, *Acta Crystallogr. Sect. C: Struct. Chem.*, 2015, **71**, 3-8.
53. O. V. Dolomanov, L. J. Bourhis, R. J. Gildea, J. A. K. Howard and H. Puschmann, *J. Appl. Crystallogr.*, 2009, **42**, 339-341.
54. Amsterdam Density Functional (ADF 2019) Code, Vrije Universiteit: Amsterdam, The Netherlands. Available at: http://www.scm.com).
55. A. D. Becke, *Phys. Rev. A*, 1988, **38**, 3098-3100.
56. J. P. Perdew, *Phys. Rev. B*, 1986, **33**, 8822-8824.
57. S. Grimme, S. Ehrlich and L. Goerigk, *J. Comput. Chem.*, 2011, **32**, 1456-1465.
58. L. Versluis and T. Ziegler, *J. Chem. Phys.*, 1988, **88**, 322-328.
59. R. van Leeuwen and E. J. Baerends, *Phys. Rev. A*, 1994, **49**, 2421-2431.
60. A. Muñoz-Castro, *Inorg. Chem. Front.*, 2019, **6**, 2349-2358.
61. T. Ziegler and A. Rauk, *Theor. Chim. Acta*, 1977, **46**, 1-10.
62. M. v. Hopffgarten and G. Frenking, *Wiley Interdiscip. Rev. Comput. Mol. Sci.*, 2012, **2**, 43-62.